Membrane lipid remodeling modulates γ-secretase processivity

Received for publication, April 26, 2022, and in revised form, February 6, 2023 Published, Papers in Press, February 16, 2023,
https://doi.org/10.1016/j.jbc.2023.103027

Edgar Dawkins[1], Rico J. E. Derks[2], Martina Schifferer[3,4], Johannes Trambauer[1], Edith Winkler[1], Mikael Simons[3,4,5], Dominik Paquet[4,6], Martin Giera[2], Frits Kamp[1], and Harald Steiner[1,3,*]

From the [1]Division of Metabolic Biochemistry, Faculty of Medicine, Biomedical Center (BMC), LMU Munich, Munich, Germany; [2]Center for Proteomics & Metabolomics, Leiden University Medical Center (LUMC), Leiden, The Netherlands; [3]German Center for Neurodegenerative Diseases (DZNE), Munich, Germany; [4]Munich Cluster of Systems Neurology (SyNergy), Munich, Germany; [5]Institute of Neuronal Cell Biology, Technical University Munich, Munich, Germany; [6]Institute for Stroke and Dementia Research, University Hospital, LMU Munich, Munich, Germany

Reviewed by members of the JBC Editorial Board. Edited by Elizabeth Coulson

Imbalances in the amounts of amyloid-β peptides (Aβ) generated by the membrane proteases β- and γ-secretase are considered as a trigger of Alzheimer's disease (AD). Cell-free studies of γ-secretase have shown that increasing membrane thickness modulates Aβ generation but it has remained unclear if these effects are translatable to cells. Here we show that the very long-chain fatty acid erucic acid (EA) triggers acyl chain remodeling in AD cell models, resulting in substantial lipidome alterations which included increased esterification of EA in membrane lipids. Membrane remodeling enhanced γ-secretase processivity, resulting in the increased production of the potentially beneficial Aβ37 and/or Aβ38 species in multiple cell lines. Unexpectedly, we found that the membrane remodeling stimulated total Aβ secretion by cells expressing WT γ-secretase but lowered it for cells expressing an aggressive familial AD mutant γ-secretase. We conclude that EA-mediated modulation of membrane composition is accompanied by complex lipid homeostatic changes that can impact amyloidogenic processing in different ways and elicit distinct γ-secretase responses, providing critical implications for lipid-based AD treatment strategies.

Recent advances in lipidomics have revealed that cellular membranes are far more complex and dynamic than previously appreciated (1). Each type of intracellular membrane, and regions thereof, are kept within specific biophysical parameters to facilitate protein and cellular function (2, 3). For example, the acyl chain composition of a lipid bilayer has influence on the packing, thickness, fluidity, and lateral pressure of membranes, which in turn has direct effects on membrane proteins and organelle functions (3–5). Disturbances to cellular membrane properties are proposed to be "sensed" by membrane sensor proteins, which elicit corrective homeostatic responses resulting in altered membrane composition (6, 7). It is currently unclear to what extent membrane biophysical parameters can be modified within existing metabolic pathways and if such mechanisms could be exploited to target membrane metabolism and modify biological function in disease.

Interestingly, many lines of evidence suggest mechanistic links between the pathogenesis of Alzheimer's disease (AD) and lipid metabolism (8, 9). In AD, patients develop amyloid plaques in the brain over a period of 15 to 20 years (10). Amyloid plaques are formed by the gradual deposition of aggregated amyloid-β peptide (Aβ). The biochemical production of Aβ occurs at the lipid membrane; thus, many studies have observed that lipids can influence Aβ generation (9). Furthermore, many of the genes associated with increased sporadic AD risk have functions in lipid metabolism (11).

Aβ is generated from the β-amyloid precursor protein (APP), which is cleaved first by β-secretase ("shedding") and then repeatedly cleaved by γ-secretase in the membrane to produce short secreted Aβ peptides of 37 to 43 amino acids in length (12). γ-Secretase is an intramembrane protease complex consisting of four subunits; nicastrin, APH-1 (a or b), PEN-2, and the catalytic subunit presenilin (PS1 or PS2). Mutations in presenilin cause autosomal dominant familial AD (FAD) by increasing the relative production of longer Aβ isoforms (Aβ42 and/or Aβ43) over the predominant Aβ40 form (12). As these long forms of Aβ are hydrophobic and more aggregation prone, the ratio of Aβ42/Aβ40 has long been considered to determine the extent to which Aβ forms amyloid plaques in patients and contribute to disease onset (13, 14). Furthermore, shorter forms of Aβ, such as Aβ37 and Aβ38, have recently been shown to slow the aggregation of longer Aβs and Aβ38 has also been associated with improved clinical progression in AD (15, 16). For this reason, targeting γ-secretase to reduce the production of longer forms of Aβ and increase shorter forms of Aβ represents a promising therapeutic strategy for AD (17).

As γ-secretase cleaves its substrates inside the membrane, its activity is critically dependent on the lipid composition of its surrounding bilayer (18–20). In assays utilizing purified γ-secretase reconstituted in proteoliposomes of defined lipid

* For correspondence: Harald Steiner, harald.steiner@med.uni-muenchen.de.

composition, we found that increasing membrane thickness can reduce the production of total Aβ and of pathogenic long species of Aβ (20). To attempt to translate these findings, we set out to investigate whether it was possible to increase membrane thickness in mammalian cells and potentially modify the pathogenic γ-secretase activity.

Under standard cell culture conditions, *de novo* fatty acid (FA) synthesis is downregulated and cells source the majority of FAs from the culture medium (21). Exogenous FAs can be utilized for β-oxidation, esterified into triglycerides (TGs), and/or incorporated into membrane lipids by the remodeling enzymes of the Lands' cycle (22–24). In the present study, we investigated if supplementing cells with very long-chain FAs (VLCFA) would increase the proportion of long-chain phospholipids and hence increase membrane thickness. The effect of this treatment and the resulting lipid modifications were then assessed by analyzing APP processing and γ-secretase activity. Our data show extensive lipidome remodeling in cells supplemented with erucic acid (EA), leading to observable incorporation of VLCFA in cellular membranes as well as altered function of WT and FAD mutant γ-secretase, resulting in altered APP processing and increased secretion of Aβ37 and/or Aβ38.

Results

Supplementation of exogenous very long-chain FA results in substantial lipidome remodeling and in activation of lipid homeostatic processes

To attempt to increase membrane thickness in a cellular system expressing PS1/γ-secretase, we supplemented HEK293 cells overexpressing Swedish mutant APP (APPsw) and PS1 (PS1 WT cells) with EA complexed to bovine serum albumin (BSA) at a molar ratio of 1:2 (BSA:EA). PS1 WT cells were incubated with BSA:EA complexes at a final EA concentration of 100 to 200 μM for 72h, in the presence of 10% fetal calf serum (FCS), with the aim of allowing incorporation of the exogenous FA into cellular phospholipids (Fig. 1*A*). Under these conditions, there was no appreciable loss in viability due to the EA treatment, although at the 200 μM concentration the high amount of BSA reduced cellular growth independently of EA treatment (Fig. S1*A*).

To investigate if EA was incorporated into cellular lipids, cells were collected and the lipids were extracted. TLC analysis of the extracted cellular lipids suggested that EA was effectively incorporated into cellular phospholipids in a dose-dependent manner, as we observed decreased retention of phospholipids on the TLC plate (Fig. 1*B*). The remodeled phospholipids migrated faster than the palmitoyl oleoyl phosphatidyl choline standard (Fig. 1*B*, lane 3), but not quite as quickly as the di-acyl chain standards (di22:1 phosphatidylcholine (PC) and di24:1 PC; Fig. 1*B*, lane 1 and 2), suggesting that there may be other species of 22:1-containing lipids generated. To determine the degree of EA incorporation in more detail, cellular extracts were extensively analyzed using a LC-MS lipidomics method to quantitatively assess acyl chain composition of the cellular lipids. Overall, EA supplementation (100 μM) resulted in about 12.0 mol% of total membrane lipids containing at least one acyl chain with 22 carbons (Fig. 1*C*), which was an increase of 8.2 mol% compared to the BSA vehicle control. Concomitantly to the membrane lipid remodeling, the storage TG and cholesterol ester (CE) lipids also showed a very strong increase to about 54.0 mol% containing acyl chains with 22 carbons (Fig. 1*C*), which is a homeostatic storage response to excess FA.

The membrane remodeling was consistent with the action of specific acyltransferases. Looking at individual lipid species, the 22:1 acyl chains were mostly incorporated into mixed acyl chain membrane and storage lipids (Figs. 1, *D* and *E* and S1, *B* and *C*). The most significantly increased individual species (fold changes) were storage TGs with 22:1 acyl chains (Fig. 1*D*) and the most significantly decreased (fold change) individual species were common membrane lipids containing 18C and 16C acyl chains (Fig. 1*D*). It was also apparent that the 22:1 acyl chains were not evenly incorporated into all membrane lipid classes (Fig. 1, *D–F*). Considering the relative amount within each lipid class (class mol%), the storage lipids, lysophospholipids, and the membrane lipid PS had the biggest proportional increase in species containing 22:1 acyl chains (Fig. 1, *E* and *F*). Thus, our lipidomic data capture a metabolic state, where membrane lipid remodeling and membrane homeostasis are activated in response to the increased amount of EA in the medium.

While advances in lipidomic technology have allowed the detailed measurement of thousands of species of lipids, it can be challenging to interpret these data due to the bulk effects of lipids in a membrane. To predict possible biophysical and cellular effects on the membrane properties as result of the lipidome remodeling, we analyzed the lipidomic data using lipid ontology analysis (25). The properties which were most significantly associated with the altered lipidomes upon EA treatment are listed (Figs. 1*G* and S1*D*). Notably, ontology terms such as "C22:1", "lipid storage," and "lipid droplet" were significantly associated with the lipids that were increased in the remodeled cells (Fig. 1*G*). Furthermore, the term "very high bilayer thickness" was significantly up, while the terms "low bilayer thickness" and "average bilayer thickness" were significantly down (Figs. 1*G* and S1*D*). Thus, the properties of the lipidome assigned by the LION algorithm indicate an activation of lipid homeostatic mechanisms and membrane remodeling.

Supplementation of EA results in alteration of observed ER membrane thickness and formation of lipid droplets

The lipidomic analysis showed that EA supplementation resulted in extensive lipid remodeling, causing a large increase in the amount of VLCFA-containing lipids in the cellular lipidome. However, as the acyl chain composition of intracellular membranes is highly regulated, these lipids may be distributed within intracellular membranes to differing extents, whereas γ-secretase activity is mostly localized in the plasma membrane (PM) and the endosomal/lysosomal compartments (26–28). Therefore, to investigate if the EA supplementation and subsequent incorporation into phospholipids resulted in

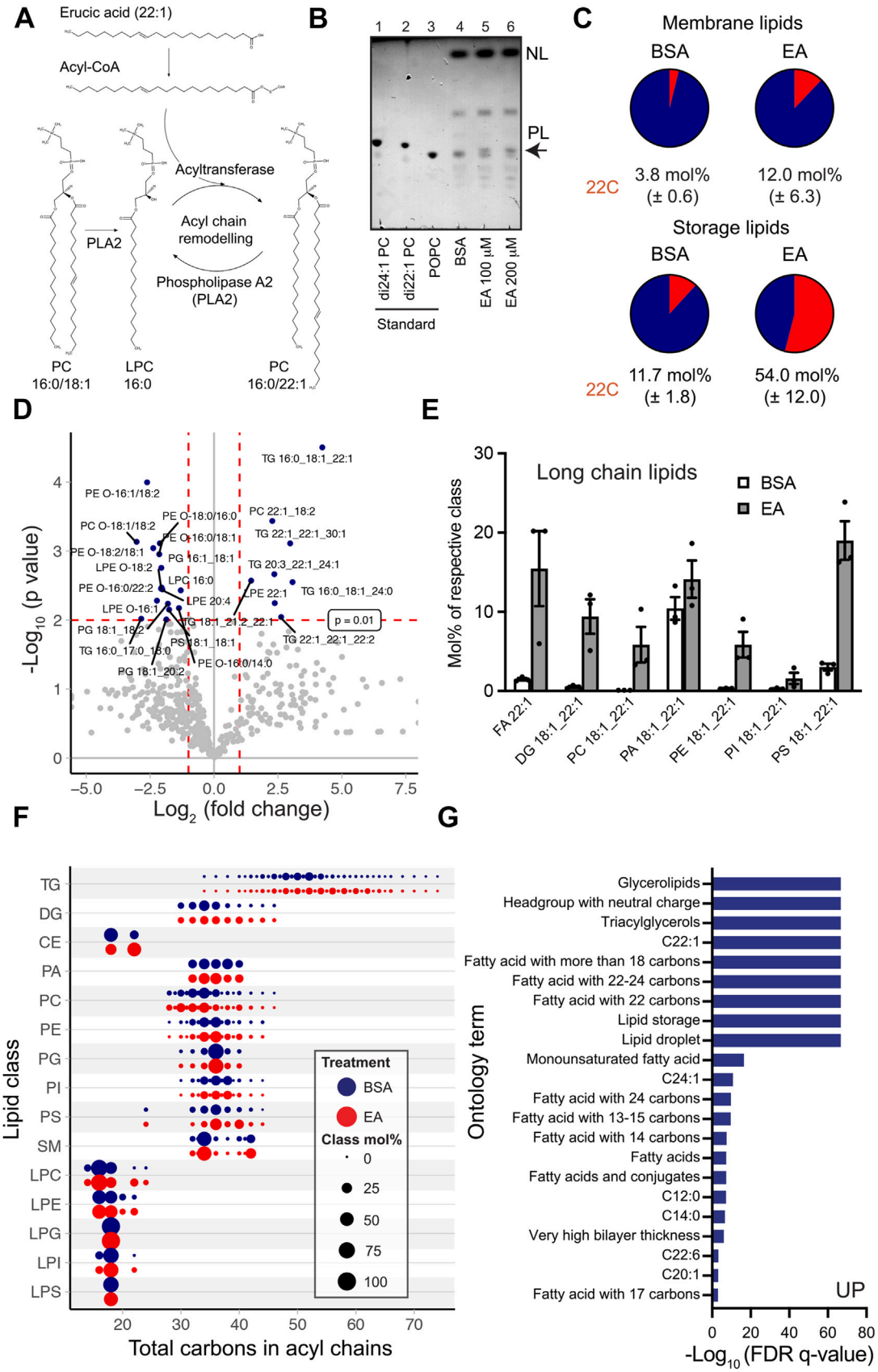

Figure 1. Lipidomic analysis of membrane lipid remodeling. *A*, scheme showing lipid remodeling Lands' cycle for 16:0/18:1 PC and the structure of erucic acid. *B*, TLC of lipid extracts from PS1 WT cells supplemented with 100 μM EA for 72 h. PL = phospholipids (mostly PC), NL = neutral lipids. *Arrow* indicates incorporation of VLCFA into the PL due to EA supplementation. *C*, pie charts depicting the molar percentage (mol%) of lipids containing at least one 22C acyl chain determined by LC-MS-based lipidomics analysis of PS1 WT cells supplemented with 100 μM EA for 72 h. Value is mean (±SD) of n = 3

an actual increase in membrane thickness, we measured the thickness of the PM and the endoplasmic reticulum (ER) of the cells by transmission electron microscopy (TEM). At low magnification, the cells treated with EA showed an expected increase in the amount of lipid droplets (Fig. 2*A*), which we confirmed by confocal microscopy using a neutral lipid stain (Fig. 2*B*). This observation was consistent with the large increase in TG/CE species containing 22:1 acyl chains measured in the lipidomics analysis. Using higher (300,000×) magnification, we were able to resolve both leaflets of the ER and the PM (Fig. 2, *A* and *C*) and measure the membrane thickness using analysis of density profiles (Fig. 2*D*). In untreated cells, the PM was significantly thicker (47.9 ± 3.16 Å, mean ± SD) than the ER (41.2 ± 3.23 Å), which is consistent with the previously reported difference in thickness between these membranes that was first observed in the 1960s (29). Remarkably, cells supplemented with EA showed a significant increase in the thickness of the ER membrane to 45.5 ± 3.52 Å (Fig. 2*D*) and a smaller increase in the PM membrane thickness to 49.2 ± 3.88 Å ($p = 0.13$). These data demonstrated that the observed lipidome remodeling resulted in increased thickness of the lipid-rich ER membranes. However, for the PM, which is much more protein and cholesterol rich, the treatment effect was less pronounced.

APP processing and Aβ generation is activated in membrane-remodeled cells

Our previous study (20) showed that purified γ-secretase activity is beneficially modified when hydrophobic thickness is increased by ≈10 Å, resulting in decreased total Aβ production and a reduced Aβ42/Aβ40 ratio. The TEM analysis suggested the EA supplementation also alters the membrane thickness in cells but not so much in the PM compartment, a major site of γ-secretase activity. Despite this, when analyzing APP processing (Fig. 3*A*) by immunoblotting and specific immunoassays, our EA treatment unexpectedly led to a dose-dependent increase in secreted total Aβ in PS1 WT cells (Fig. 3*B*).

With further examination, it was observed that the levels of sAPPα and sAPPβsw were also increased, with a stronger effect on β-secretase cleavage (Fig. 3, *C* and *D*), which suggested membrane remodeling led to a stimulation of APP processing in general. Analysis of the cell lysates demonstrated that the levels of full-length APP, PS1, and nicastrin were unchanged by the treatment (Fig. 3*E*) but the levels of APP CTFs were slightly increased (Fig. 3*E*). Therefore, the data suggested that there were activation effects of membrane remodeling on the α- and β-secretase–mediated shedding steps of APP processing.

To further demonstrate that the increased Aβ secreted by the EA-treated cells was not caused by an effect on γ-secretase, the ratio of Aβ to sAPPβsw in the medium was analyzed. This ratio should reflect the extent to which APP C-terminal fragment CTFβ is cleaved by γ-secretase and account for changes in cellular secretion, growth etc. The Aβ/sAPPβsw ratio was not changed in the PS1 WT expressing cells upon EA treatment (Fig. 3*F*), suggesting no increased cleavage by γ-secretase.

Finally, to address the direct effects on γ-secretase and exclude the effect of lipids on APP shedding, the effect of EA treatment was investigated on HEK293 cells stably coexpressing C99-6myc and F-NEXT (30), *i.e.*, truncated forms of the APP CTFβ and Notch1 that are direct substrates for γ-secretase. In these cells, there was no significant increase in the total amount of Aβ secreted (Fig. S2*A*). Furthermore, there were no clear effects on the amount of the intracellular domains APP intracellular domain or notch intracellular domain generated relative to the precursors C99-6myc and F-NEXT (Fig. S2, *B*–*D*). Collectively, the data demonstrated that EA lipid treatment activates APP processing, resulting in more APP CTFs and subsequent production of Aβ but did not indicate any direct effects on the total amount of APP CTF cleavage by γ-secretase itself.

Membrane lipid remodeling modulates γ-secretase and increases short forms of Aβ

Our earlier *in vitro* study showed that increased membrane thickness not only inhibited Aβ production but also modulated the ratio of Aβ species produced (20). Therefore, the effect of VLCFA incorporation in the membrane lipids on Aβ ratios was also evaluated in lipid-remodeled PS1 WT cells. The Aβ42/Aβ40 ratio, which is implicated in AD pathogenesis, reflects two main mechanistic features of γ-secretase cleavage (12). Firstly, CTFβ cleavage can occur along two product lines, referred to as the Aβ40 product line and the Aβ42 product line (Fig. 4*A*). Secondly, once positioned in a product line, the substrate is sequentially cleaved by γ-secretase ≈ every 3 amino acids (Fig. 4*A*). The extent to which this sequential cleavage occurs is referred to as processivity and can influence the observed Aβ42/Aβ40 ratio.

To determine the effect of EA supplementation on γ-secretase product lines and processivity, the production of various Aβ species was measured by ELISA. In the PS1 WT cells, EA supplementation dose-dependently reduced the AD ratio (Aβ42/Aβ40) by a small nonsignificant extent (Fig. 4*B*). However, this was not consistently observed in all cell types examined in this study. In the induced pluripotent stem cell (iPSC)-derived cortical neurons which do not overexpress APP, there was a larger significant reduction in the Aβ42/Aβ40 ratio (Fig. 4*D*) but in the cells overexpressing the C99-6myc construct there was no such effect (Fig. S2*E*). Likewise, there

independent experiments. Membrane lipids are defined as all measured lipids except FA, TG, and CE. Storage lipids are defined as TG and CE. *D*, volcano plot of lipidomic data showing mean fold changes from n = 3 independent experiments with PS1 WT cells supplemented with 100 μM EA for 72 h. *E*, bar graph of lipidomic data showing selected altered lipid species in PS1 WT cells supplemented with 100 μM EA for 72 h. Bars show mean ± SEM mol% per class from n = 3 independent experiments. *F*, bubble plot showing total number of carbons in acyl chains of major lipid classes from PS1 WT cells supplemented with 100 μM EA for 72 h. Area of bubble corresponds to mean class mol% of each species from n = 3 independent experiments. *G*, LION ontology analysis of lipidomic data generated from n = 3 independent experiments with PS1 WT cells supplemented with 100 μM EA for 72 h showing associated terms upregulated *versus* BSA control with a false discovery rate threshold of $q < 0.05$. BSA, bovine serum albumin; CE, cholesterol ester; FA, fatty acid; PC, phosphatidylcholine; PS1, presenilin1; TG, triglyceride; VLCFA, very long-chain fatty acid.

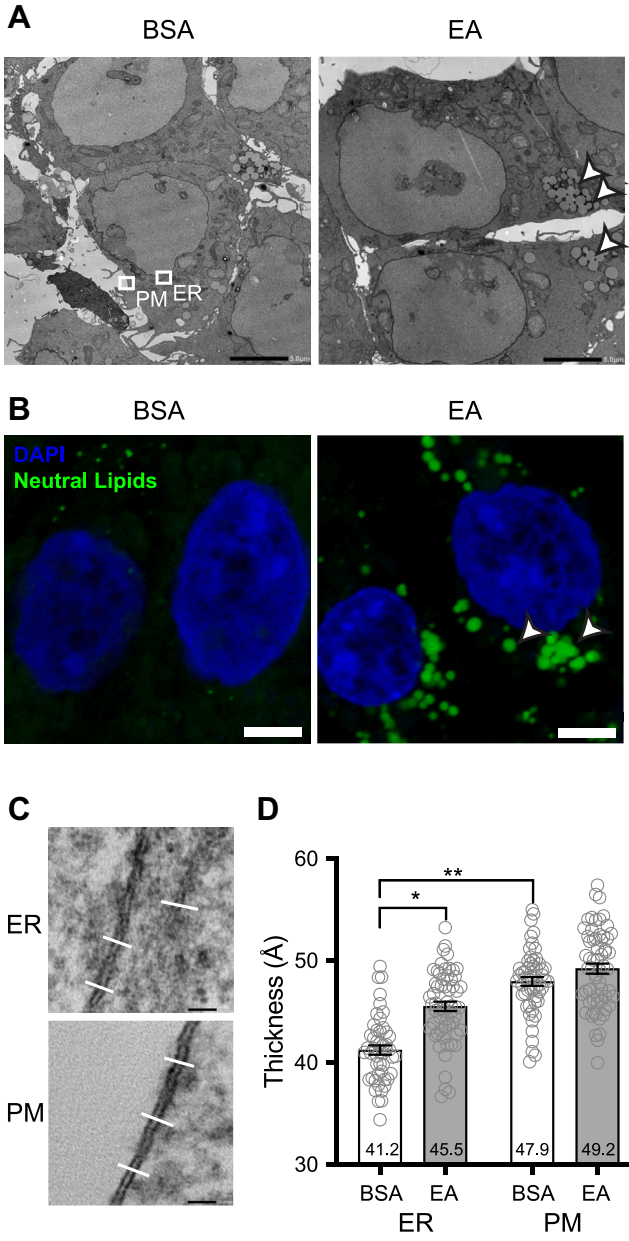

Figure 2. EA supplementation modifies membrane thickness and lipid storage. *A*, TEM images at 40,000× magnification of PS1 WT cells treated with EA (100 μM) for 72 h. *Arrows* highlight accumulation of lipid droplets. *White boxes* give examples of ER and PM regions which were used for analysis of density profiles. The scale bar represents 5 μm. *B*, confocal images of PS1 WT cells stained with LipidTOX neutral lipid stain and DAPI, treated with EA (100 μM) for 72 h. The scale bar represents 5 μm. *C*, examples of 300,000× magnification images of PM and ER membranes which were used to generate density profiles for measurement of membrane thickness. Examples of transects are shown by *white lines*. The scale bar represents 20 nm. *D*, measurement of membrane thickness from 546 measured membrane transects from n = 3 independent experiments of cells treated with 100 μM EA for 72 h. Bars show mean ± SEM. *Asterisks* indicate p values < 0.05 determined by two-tailed nested paired t test. Mean values are specified in each column. DAPI, 4′,6-diamidino-2-phenylindole; EA, erucic acid; ER, endoplasmic reticulum; PM, plasma membrane; PS1, presenilin1; TEM, transmission electron microscopy.

was no effect on the AD ratio in the near-haploid human cell line HAP1 (Fig. S3*A*). Thus, EA supplementation has a differential magnitude of effect on the AD ratio, depending on the cell type.

The AD ratio, although historically used as a proxy for disease relevance, does not fully consider the complexity of γ-secretase activity (Fig. 4*A*). When examining shorter Aβ species as well, we observed an obvious increase in the relative proportion of Aβ38 induced by the membrane remodeling (Fig. 4*C*). This Aβ38 modulation effect was also observed in WT human iPSC-derived cortical neurons (Fig. 4*D*), in the cells expressing the truncated C99-6myc construct (Fig. S2*F*) and to a lesser extent in HAP1 cells (Fig. S3*B*). These data demonstrated that the increase in Aβ38 caused by EA supplementation occurs in different cell types including neurons and in the absence of full-length APP or PS1 overexpression.

To investigate if the lipid remodeling affected the processivity of γ-secretase cleavage along the product lines, we measured the products of the last cycles of Aβ cleavage by examining the ratio of Aβ38/Aβ42 (Aβ42 product line processivity) and the ratio of Aβ37/Aβ40 (Aβ40 product line processivity). This analysis demonstrated that the EA treatment significantly increased the processivity of both product lines (Figs. 4, *D–F*, S2*G*, and S3*C*). For the PS1 WT cells and the iPSC-derived cortical neurons the Aβ38/Aβ42 ratio was even doubled (Fig. 4, *D* and *E*).

Familial AD PS1 mutants are differentially affected by membrane lipid remodeling

In parallel to the investigation in PS1 WT cells, where Aβ production was stimulated and the increased Aβ38 secretion was observed, the effect of EA was also investigated in cells expressing the PS1 FAD mutations PS1 Δexon9 (PS1 Δ9) and PS1 L166P. Similar to PS1 WT, Aβ secretion in the PS1 Δ9 mutant cells was stimulated by the EA supplementation (Fig. 5*A*). However, remarkably, in the cells expressing PS1 L166P the secretion of Aβ was reduced upon EA supplementation (Fig. 5*A*). The decrease in Aβ secretion occurred even though the shedding of APP was increased, as shown by the levels of sAPPα and sAPPβsw and with a relative preference of α-secretase cleavage for the PS1 L166P mutant (Fig. 5, *B* and *C*). Additionally, the expression of full length APP (APP FL) and γ-secretase remained the same (Fig. 5*D*). However, upon EA treatment the PS1 L166P mutant had an accumulation of APP CTFs [APP CTFs/APP FL = 0.70 (200 μM EA), Fig. 5, *D* and *E*] which was stronger than the WT [APP CTFs/APP FL = 0.22 (200 μM EA, Fig. 3*E*)] and showed a decreased Aβ/sAPPβsw ratio (Fig. 5*F*). Both of these measures indicate a reduction in γ-secretase cleavage of APP CTFβ.

In both mutants there were very slight decreases in the Aβ42/Aβ40 ratio (Fig. 5*G*), similar to the PS1 WT (Fig. 4*B*). However, the effects on processivity were not the same as the PS1 WT and were different for each mutant. The Aβ42 product line processivity was only significantly changed for the PS1 L166P at the 100 μM concentration (Fig. 5*H*), and the Aβ40 product line processivity was higher in the PS1 Δ9 mutant at the 200 μM concentration but very slightly lower in the PS1 L166P mutant (Fig. 5*I*). Collectively, these data unexpectedly show that the PS1 FAD mutant expressing cells

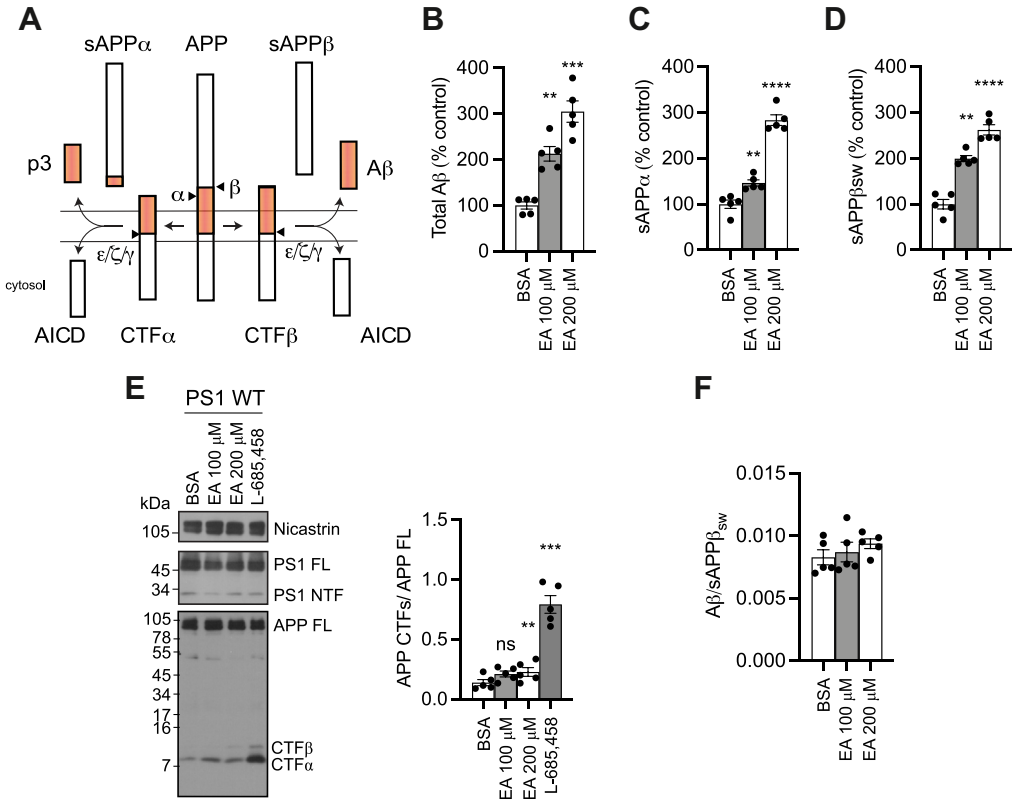

Figure 3. Effect of membrane remodeling on APP processing. *A*, scheme of APP processing, showing products of α-, β-, and γ-secretase (ε, ζ, γ) cleavages. *B*, PS1 WT cells were incubated with EA or BSA vehicle for 72 h, before the medium was replaced and conditioned medium was collected for 5 h. Secreted Aβ was measured by ELISA. Bars show mean ± SEM from n = 5 independent experiments. *C*, secreted sAPPα in the medium as measured by ELISA. Bars show mean ± SEM from n = 5 independent experiments. *D*, secreted sAPPβsw in the medium as measured by ELISA. Bars show mean ± SEM from n = 5 independent experiments. *E*, expression of PS1, nicastrin, and APP in RIPA lysates of cells measured by immunoblotting. L-685,458 (1 μM) was included in the indicated condition. Right graph shows quantification of ratio of APP CTFs to APP FL from immunoblot analysis. Bars show mean ± SEM from n = 5 independent experiments. *F*, Aβ/sAPPβsw ratio in the medium determined by ELISA measurement. Bars show mean ± SEM from n = 5 independent experiments. In *B–F*, *asterisks* indicate *p* values < 0.05 *versus* BSA control by two-tailed paired *t* test. APP, amyloid precursor protein; APP FL, full length APP; BSA, bovine serum albumin; CTF, C-terminal fragment; EA, erucic acid; FL, full length; NTF, N-terminal fragment; PS1, presenilin1.

display divergent responses to the EA-induced membrane remodeling when compared to the PS1 WT expressing cells.

Discussion

Our earlier study (20) determined that γ-secretase activity in proteoliposomes can be modified by a thicker membrane lipid environment; therefore, the initial aim of this study was to examine to what extent it is possible to thicken the membrane of living mammalian cells. We took advantage of the fact that in normal metabolism cells constantly exchange acyl chains of membrane lipids through the Lands' cycle (31). After investigating an alternative method (32), we found BSA:EA complexes to be particularly effectively incorporated into many cellular lipids.

Interestingly, EA was not equally incorporated into all classes of membrane lipids, but some classes more than others, which probably reflects the action of a specific acyltransferase(s). Importantly, the acyltransferases that catalyze the remodeling of membrane lipids display donor and recipient specificity, which is thought to regulate the overall acyl chain composition of various membranes (33, 34). To our knowledge, it is not known which specific acyltransferase catalyzes the incorporation of EA (34). Concomitant to the observed membrane lipid remodeling, the storage lipids (TG and CE) also showed a major increase to about 54% of these species containing 22 carbon acyl chains. These data suggest that a large proportion of the exogenous EA is directed to lipid droplet stores as a homeostatic mechanism, while a smaller proportion is incorporated through acyl chain remodeling pathways into membrane lipids.

Despite the extensive acyl chain remodeling observed by lipidomics, with dramatic EA incorporation in particular membrane lipids, the overall increase of C22 FAs in total membrane lipids was only to 12 mol%, so it was not clear if this would actually result in an observable thickening of cellular membranes. Using TEM, it was possible to measure membrane thickness and to validate the difference in thickness between the ER and the PM, which was first reported around the 1960s (29, 35). In EA-treated cells, a large thickness change was measured in the ER and the PM thickness increase was small. These data may reflect the fact that many of the acyltransferases are located in the ER (24) and the PM is subject to a number of other homeostatic regulatory mechanisms that may counteract the excess 22 carbon-containing membrane lipids. Alternatively, the observed electron density of the PM may be influenced by

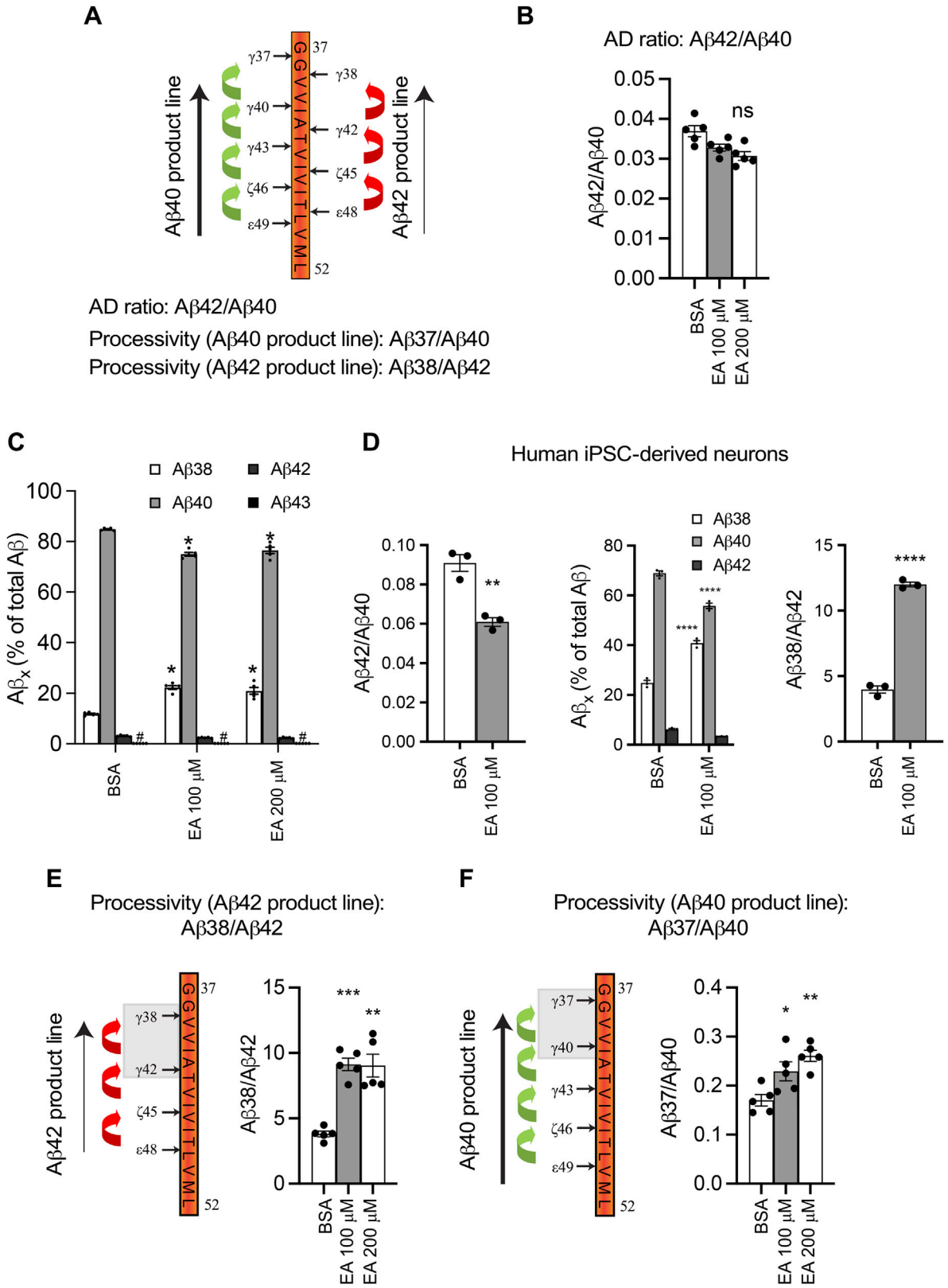

Figure 4. EA supplementation modulates γ-secretase processivity. *A*, scheme showing processive substrate cleavage of APP CTF by γ-secretase and product lines. The Aβ40 producing line is shown with a *thick arrow* as this is the major product line. Cleavage and amino acid residue numbers are shown for CTFβ. *B*, Aβ42/Aβ40 ratios from medium collected from PS1 WT cells treated with the indicated concentrations of EA for 72 h, prior to collection of medium for 5 h, measured by ELISA. Bars show mean ± SEM from n = 5 independent experiments. ns = $p > 0.05$ *versus* BSA control by two-tailed paired *t* test. *C*, Aβ ratios measured by ELISA from PS1 WT cells. Bars show mean ± SEM from n = 5 independent experiments. *Asterisks* indicate *p* values < 0.05 *versus* BSA control by two-way ANOVA with Tukey multiple comparisons test. (#) Note Aβ43 measurements are not visible on graph due to low value. *D*, Aβ ratios measured in DIV30 iPSC-derived cortical neurons, treated with 100 μM EA or BSA vehicle 96 h prior to collection and analysis of medium by MSD ECL-IA. Bars show mean ± SEM from 3 replicate wells. Representative experiment of n = 2 independent differentiations. *Asterisks* indicate *p* values < 0.05 *versus* BSA

the protein- and cholesterol-rich nature of this membrane compared to the ER (36). TEM has the important caveat that the observed thicknesses do not represent the true value, due to the effects of the fixatives and staining processes on membrane structure. However, these data demonstrate that membrane lipid remodeling in cells results in observable changes to the structure of the membrane, which must reflect changes to biophysical properties of the membrane such as altered thickness, packing, fluidity, and raft formation.

Importantly, as APP processing by γ-secretase occurs in late secretory pathway compartments and the PM, this may imply that our strategy to remodel membranes and increase membrane thickness would have a minimal effect on its activity. Considering this fact, we were surprised to observe that membrane remodeling resulted in relatively more Aβ37 and Aβ38 secreted than longer Aβ isoforms, which can only be explained by an effect of the membrane remodeling on γ-secretase itself. This enhanced processivity of γ-secretase upon EA supplementation was replicated in cells expressing the C99-6myc construct and in the absence of APP overexpression in human iPSC-derived cortical neurons and HAP1 cells. These consistent effects caused by elevated levels of VLCFA in cellular membranes are in agreement with our earlier study of γ-secretase reconstituted in model membranes of defined thickness (20).

Whereas in model membranes an inhibition of γ-secretase was observed in thicker membranes, cellular data showed an unexpected increase in total secreted Aβ upon EA supplementation. However, this was due to elevated APP cleavage by β-secretase rather than an effect on γ-secretase. Surprisingly, although the EA treatment had similar stimulatory effects on APP processing for the PS1 Δ9 mutant and PS1 WT, we found that for the PS1 L166P mutant it had a dose-dependent inhibitory effect on the secretion of Aβ. This difference might have been caused by a composite effect due to a relative increase of α-secretase over β-secretase cleavage as well as by an inhibition of PS1 L166P γ-secretase. The PS1 L166P mutant has previously been reported to have a differential localization within the cell (26), which could possibly contribute some of the differential effects we observed. Interestingly, we noted that EA treatment caused an increase of WT and L166P mutant γ-secretases in the late endosomal/lysosomal compartments but this had divergent effects on Aβ levels (unpublished observations). This puzzling observation will require deeper future research to be understood. Of note, the phenomenon of decreased production of Aβ from its precursor CTFβ has important implications for the use of AD mouse models, as the PS1 L166P mutation is used to induce AD-like pathology for example in the APPPS1 mouse (37). In particular, drugs or lipid dietary approaches tested in L166P-expressing model systems may give false positive results or contradictory results to other model systems and humans due to this effect. It is also possible that other commonly used AD phenotype-inducing PS1 mutations could display similar lipid-stimulated effects, which should be a consideration for preclinical studies. From the two PS1 mutants considered here, we conclude the responses to a lipid treatment are complex and cannot be expected to correspond to the PS1 WT, which is found in the majority of AD patients.

Recent studies suggest that the increased Aβ37 and Aβ38 induced by lipid membrane remodeling could be theoretically beneficial to AD pathogenesis. Emerging data suggest that even small amounts of Aβ37 and Aβ38 reduce the ability of Aβ42 to aggregate (15). Aβ37 and Aβ38 can ameliorate the phenotypes of degeneration models, possibly by reducing the amyloidogenic potential of longer Aβs (15, 38, 39). Higher cerebrospinal fluid Aβ38 has recently even been shown to be associated with reduced cognitive decline in AD patients (16). Furthermore, the ratios of short Aβ species to long Aβ species are better predictors of disease onset than the traditionally used Aβ42/Aβ40 ratio (40, 41). These new studies highlight that γ-secretase modulating strategies which increase shorter Aβ isoforms have enormous potential as AD treatments and warrant clinical evaluation.

Numerous studies have shown that interfering with lipid homeostasis by various mechanisms, including supplementation with FAs, can affect the production of Aβ (reviewed in (9)). Our data suggest that the membrane remodeling induced by a VLCFA has direct effects on the proteases implicated in Aβ production as well as on γ-secretase processivity. Therefore, our study and others collectively implicate a general effect of cellular lipid homeostasis on amyloid generation by γ-secretase. In principle, modifying the acyl chain composition of cellular membranes could provide a basis for the further development of a dietary preventative strategy for AD. However, the data in our present study indicates that there may be no one-size-fits-all approach and rather specific lipid-targeting interventions may have to be tailored to the genetic background of the experimental subject in question. Certainly, future preclinical experiments generated with lipid-altering approaches and AD models should carefully consider the direct interaction between Aβ production, presenilin mutations, and various lipids.

Experimental procedures

Antibodies

Antibodies to PS1 N-terminal fragment (NTF) (2G7, IB; 3 μg ml^{-1}) have been described (42). A monoclonal antibody to the APP C terminus was purchased from Abcam (Y188, ab32136, IB; 1:2000). A polyclonal antibody to the C terminus of nicastrin (N1660, IB; 1:10,000) and monoclonal antibody to actin (AC-74, IB; 1:1000) were purchased from Sigma-Aldrich. A monoclonal antibody to the c-myc epitope (9E10, IB; 1:100) was obtained from Santa Cruz Biotechnology.

control by two-tailed unpaired *t* test (*left/right graph*) and two-way ANOVA with Šidák multiple comparisons test (*middle graph*). *E* and *F*, processivity ratios by ELISA of medium collected from PS1 WT cells treated with indicated concentrations of EA. Bars show mean ± SEM from n = 5 independent experiments. *Asterisks* indicate *p* values < 0.05 *versus* BSA control by two-tailed paired *t* test. APP, amyloid precursor protein; BSA, bovine serum albumin; CTF, C-terminal fragment; EA, erucic acid; ECL, electrochemiluminescence; PS1, presenilin1.

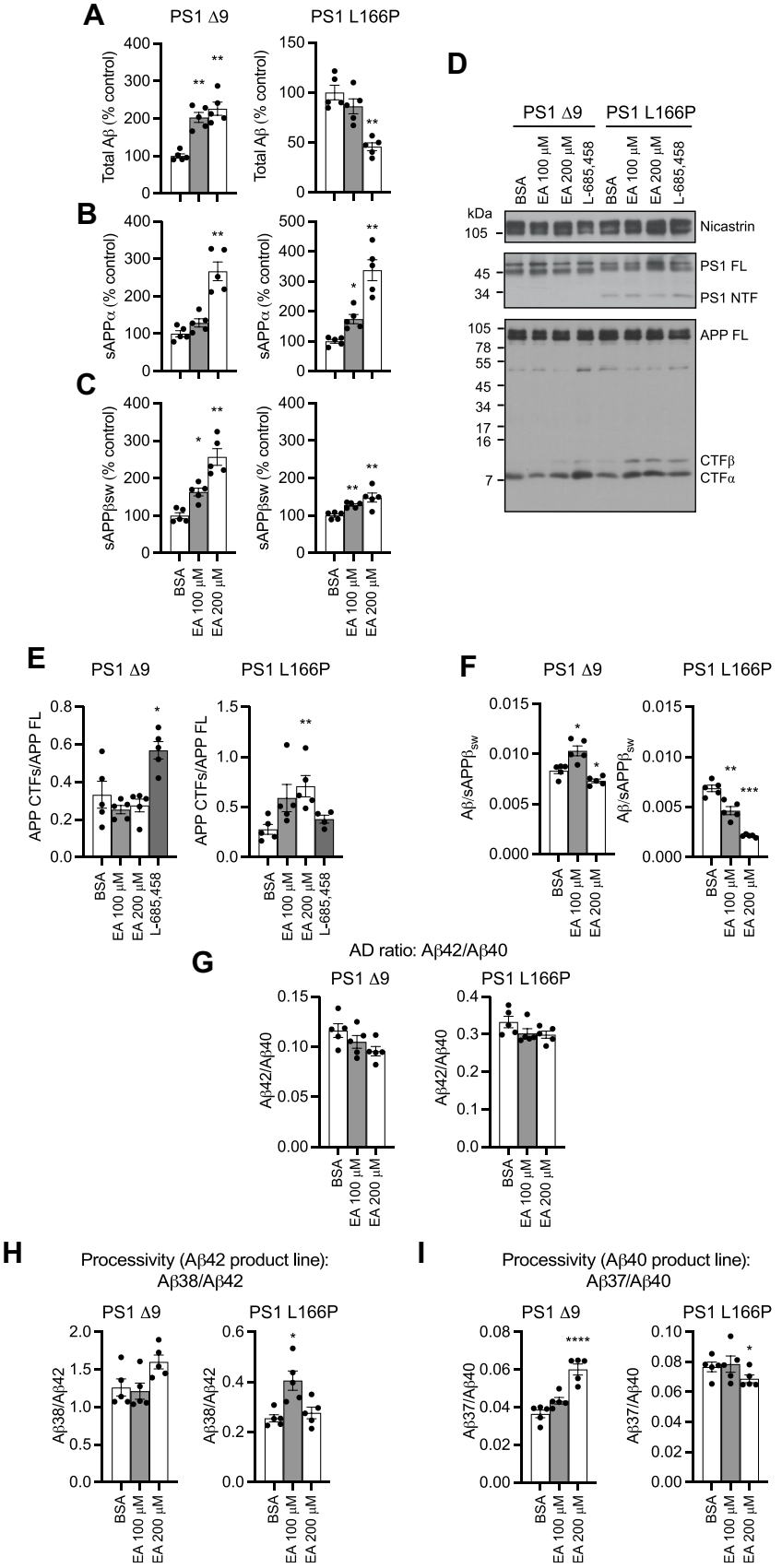

Figure 5. Differential effects of EA supplementation on Aβ generation by FAD presenilin mutants. *A*, FAD-mutant PS1 expressing cells were incubated with EA or BSA vehicle for 72 h, before the medium was replaced and conditioned medium was collected for 5 h. Secreted Aβ was measured by ELISA. Bars show mean ± SEM from n = 5 independent experiments. *B*, secreted sAPPα in the medium of FAD-mutant PS1 cells as measured by ELISA. Bars show mean ± SEM from n = 5 independent experiments. *C*, secreted sAPPβsw in the medium of FAD-mutant PS1 cells as measured by ELISA. Bars show mean ±

Cell culture

HEK293 cells stably overexpressing Swedish (sw) mutant APP (HEK293/sw) and PS1 WT (43) or PS1 Δexon9 (44) or PS1 L166P (45) and HEK293 cells stably coexpressing C99-6myc and F-NEXT cells (30) were maintained in Dulbecco's modified Eagle's medium (DMEM) containing 10% FCS, 2% L-glutamine, 1% penicillin and 1% streptomycin, and 200 μg ml^{-1} zeocin and 200 μg ml^{-1} G418. HAP1 cells (Horizon Discovery) were cultured in Iscove's Modified Dulbecco's Medium with 10% FCS, 1% penicillin, and 1% streptomycin. iPSC experiments were performed in accordance with relevant guidelines and regulations. iPSC line 7889S (46) was grown in Essential 8 Flex Medium (Thermo Fisher Scientific, A2858501) on vitronectin-coated cell culture plates (Thermo Fisher Scientific, A14700) with 5% CO_2 at 37 °C and split as small clumps twice a week after a 5 min incubation in PBS/EDTA. iPSC-derived cortical neurons were differentiated by a dual-SMAD-inhibition protocol, as described (46), and used for assays at day 30.

BSA-EA complex preparation and treatment

BSA-EA conjugates were prepared at a molar ratio of 1:2. FA free BSA (Sigma-Aldrich A8806) was dissolved to 1 mM concentration in PBS, then warmed to 37 °C, and the pH was adjusted to 7.4. The solution was filtered with a 0.4-μm syringe filter (VWR scientific). A 10 mg ml^{-1} solution of EA (FA 22:1, Sigma-Aldrich E3385) in ethanol was prepared and warmed to 37 °C. The warmed EA solution was then added dropwise with agitation to the warmed BSA solution, avoiding precipitation. Sterile 37 °C PBS was then added, so that the final concentration of BSA was 0.5 mM and the final concentration of FA was 1 mM. The BSA:EA solution was incubated at 37 °C with agitation in an orbital shaker for 1 h, before aliquots were stored at −20 °C. A vehicle control was prepared in parallel by adding an equivalent volume of ethanol to the BSA solution.

Lipid extraction and TLC

Cells were scraped and washed twice in ice-cold PBS by centrifugation at 2500*g* for 10 min at 4 °C. Twenty five to fifty percent of the cell pellet was resuspended in $CHCl_3$:MeOH (1:2). Pellets were briefly bath sonicated before centrifugation at 17,000*g* for 10 min at 4 °C. The organic phase containing cellular lipids was spotted on silica TLC plates (Millipore 1.05644.001) and resolved using a mobile phase of $CHCl_3$:MeOH:H_2O (65:25:4). Synthetic di24:1 PC, di22:1 PC, and palmitoyl oleoyl phosphatidyl choline (Avanti) were used as standards (0.5 ng). Plates were developed by spraying with 10% $CuSO_4$ (w/v) in 8% phosphoric acid (v/v) and charring at 95 °C overnight on a hot plate.

Lipidomics

Lipidomic analysis of cell lipid extracts was performed using a LC-MS/MS-based lipid profiling method. A Shimadzu Nexera LC-30 (Shimadzu) was used to deliver a gradient of water:acetonitrile 80:20 (eluent A) and water:acetonitrile:2-propanol 1:90:9 (eluent B). Both eluents contained 5 mM ammonium formate and 0.05% formic acid. The applied gradient, with a column flow of 300 μl min^{-1}, was as follows: 0 min 40% B, 10 min 100% B, 12 min 100% B. A Phenomenex Kinetex C18, 2.7 μm particles, 50 × 2.1 mm (Phenomenex) was used as column. The injection volume was 10 μl. The MS was a Sciex TripleTOF 6600 (AB Sciex) operated in positive (ESI+) and negative (ESI−) electrospray ionisation (ESI) mode, with the following conditions: ion source gas 1, 2 and curtain gas 30 psi; temperature 350 °C; acquisition range m/z 100 to 1200; IonSpray Voltage 5500 V (ESI+) and −4500 V (ESI−); and declustering potential 80 V (ESI+) and −80 V (ESI−). An information dependent acquisition method was used to identify lipids, with the following conditions for MS analysis: collision energy ±10, acquisition time 250 ms and for MS/MS analysis: collision energy ±45, collision energy spread 25, ion release delay 30, ion release width 14, and acquisition time 40 ms. The information dependent acquisition switching criteria were set as follows: for ions greater than m/z 300, which exceed 200 cps, exclude former target for 2 s, exclude isotopes within 1.5 Da, and max. candidate ions 20.

Before data analysis, raw MS data files were converted with the Reifycs Abf Converter (v1.1) to the Abf file. MS-DIAL (v2.74), with the FiehnO (VS27) database, was used to align the data and identify the different lipids (47). PC and phosphatidylethanolamine lipids were manually curated to confirm their identity. Due to overlap of TG species, MS-DIAL could not sufficiently identify lipid species, in turn a modified identification approach was applied. Initially, MS-DIAL was used to get the total number of carbons and double bonds of a TG. This information together with the MS/MS spectrum was used to search the glycerolipid MS/MS predicted database on Lipid Maps (48). TGs with all their neutral loss of lipid species fragments matched where assigned as correctly identified. Lipid ontology analysis was performed using LION, in two-tailed ranking mode using Log2 fold change local statistics (25). Species containing zero values were excluded from LION analysis.

Transmission electron microscopy

PS1 WT cells were grown on Aclar sheets (Science Services) coated with poly-L-lysine at a density of 1.1 × 10^5 cells cm^{-1} (Sigma-Aldrich) for 72 h, then fixed in 2.5% glutaraldehyde (EM-grade, Science Services) and 0.05% malachite green (Sigma Aldrich) in 0.1 M sodium cacodylate

SEM from n = 5 independent experiments. *D*, expression of PS1, nicastrin, and APP in RIPA lysates of FAD-mutant PS1 cells measured by Western blot. L-685,458 (1 μM) was included in the indicated condition. *E*, quantification of the ratio of APP CTFs to APP FL in FAD-mutant PS1 cells by immunoblotting. Bars show mean ± SEM from n = 5 independent experiments. *F*, Aβ/sAPPβsw ratio in the medium of FAD-mutant PS1 cells determined by ELISA measurement. Bars show mean ± SEM from n = 5 independent experiments. *G–I*, processivity ratios by ELISA of medium collected from FAD-mutant PS1 expressing cells treated with indicated concentrations of EA. Bars show mean ± SEM from n = 5 independent experiments. In *A–C* and *E–I*, *asterisks* indicate *p* values < 0.05 *versus* BSA control by two-tailed paired *t* test. APP, amyloid precursor protein; BSA, bovine serum albumin; CTF, C-terminal fragment; EA, erucic acid; FAD, familial Alzheimer's disease; FL, full length; NTF, N-terminal fragment; PS1, presenilin1.

buffer (pH 7.4) (Science Services). After postfixation in 1% osmium tetroxide, 0.8% potassium ferrocyanide in 0.1 M sodium cacodylate buffer and a mordant step in 1% tannic acid (Sigma Aldrich), cells were contrasted in 0.5% uranyl acetate (Science Services). After dehydration, infiltration in epon (Serva) and curing, cell monolayers were ultrathin sectioned at 50 nm thickness on formvar-coated copper grids (Plano) and postcontrasted using 1% uranyl acetate and Ultrostain (Leica). TEM images were acquired at 40,000× and 300,000× magnification on a JEM1400plus electron microscope (JEOL).

Images were collected and analyzed in a blinded fashion. Membrane thickness was measured based on previous publications (29, 49). Two to three transects of the PM or ER were generated from each 300,000× magnification image, using the ImageJ (v1.52q) density profile tool. The distance between the peak densities, corresponding to the edges of the membrane was then averaged from 15 to 20 images per experimental condition by a blinded observer, for each of the 3 experiments.

Biochemical analysis of APP processing and Aβ production

Cells were plated at a density of 1.1×10^5 cells cm^{-1} determined by trypan blue exclusion, in DMEM/FCS containing supplementary EA. Cells were grown for 72 h before medium was changed to DMEM/FCS without EA. After 5 to 6 h, the medium was collected and centrifuged at 2500*g* for 10 min prior to analysis of secreted proteins. The cells were scraped in ice-cold PBS and washed twice by centrifugation (2500*g*, 10 min). To extract cellular proteins, cells were lysed in radioimmunoprecipitation assay buffer (50 mM Tris–HCL, pH 7.4; 150 mM NaCl, 1% Triton X-100; 0.1% SDS; 0.5% sodium deoxycholate, Roche cOmplete Mini protease inhibitor cocktail). The lysate was cleared by centrifugation at 17,000*g* for 10 min. Protein levels were determined by bicinchoninic acid assay (Uptima) and the protein concentration of lysates were adjusted to equal amounts before analysis by immunoblotting. In some experiments, the γ-secretase inhibitor L-685458 (Merck, 565771) was used as a positive control.

PS1 NTF, nicastrin, Aβ, and APP CTFs were analyzed using 10 to 16.5% Tris-Tricine gradient gels (50) and transferred to nitrocellulose membranes (0.2 μm pore size; GE 1060001) which were boiled in PBS for 10 min before probing with antibodies. For quantitation of amyloid ratios, Aβ was measured by a multiplex electrochemiluminescence immunoassay (Mesoscale Discovery; (K15199E/K15200G) or by enzyme-linked immunosorbent assay (ELISA; Immuno-Biological Laboratories; RE59771, RE59791, RE59781, RE59711), following the manufacturer's protocols. sAPPα and sAPPβsw were measured by ELISA (Immuno-Biological Laboratories; JP27731, JP27733). The Aβ37/Aβ40 ratio was measured by electrochemiluminescence immunoassay as described (42).

Neutral lipid staining

Cells were plated on 12 mm poly-L-lysine coated glass coverslips at a density of 1.1×10^5 cells cm^{-1} and grown for 72 h in the presence of BSA or EA. Cells were fixed in 4 % paraformaldehyde in PBS solution for 20 min. For neutral lipid staining, coverslips were washed 2× in PBS, stained with 4′,6-diamidino-2-phenylindole in PBS (1 μg ml^{-1}), and then LipidTOX green reagent was added according to the manufacturer's protocol (Molecular Probes). Coverslips were mounted using DAKO aqueous mounting medium. Images were collected using a Zeiss LSM-800 confocal microscope.

Viability assay

Cells were plated at a density of 3×10^4 cells cm^{-1} in 96-well plates. Cells were grown in the presence of EA for 72 h prior to viability assay using the CellTiter 96 AQueous One Solution Viability assay (Promega).

Statistical analysis

Statistical analysis was performed using GraphPad Prism v. 9 (GraphPad software Inc.), RStudio v. 1.2.503 (Posit software PBC), and R v. 4.1.2 (R Core Team, 2021). Except where explicitly indicated, n refers to independent experiments performed on independent days. p values are notated as follows ns = $p > 0.05$, $^{*}p < 0.05$, $^{**}p < 0.01$, $^{***}p < 0.005$, $^{****}p < 0.0001$. Electron microscopy data were collected, randomized, and analyzed in a blinded fashion, all other experiments were performed unblinded. Sample sizes were chosen according to data from preliminary experiments and availability of experimental resources. No power calculations were conducted.

Data availability

Source data is available from the corresponding author.

Supporting information—This article contains supporting information.

Acknowledgments—The authors thank Gabriele Basset, Brigitte Nuscher, Alice Sülzen, Claudia Abou-Ajram, Lukas Feilen, and Kerstin Karg for technical advice and assistance. The authors additionally thank Anja Capell, Georg Werner, and Katrin Buschmann for helpful discussions.

Author contributions—E. D., F. K., and H. S. conceptualization; E. D., R. J. E. D., Martina Schifferer, E. W., and D. P., methodology; E. D., R. J. E. D., Martina Schifferer, J. T., and D. P., investigation; E. D. writing-original draft; R. J. E. D., Martina Schifferer, J. T., Mikael Simons, D. P., F. K., and H. S. writing-review and editing; Martina Schifferer, Mikael Simons, M. G., F. K., and H. S. funding acquisition; Mikael Simons, D. P., M. G., F. K., and H. S. resources; H. S. supervision.

Funding and additional information—This study was supported by the Deutsche Forschungsgemeinschaft (DFG) through grants ID 321765742 and ID 263531414 (FOR2290) to H. S., the Alzheimer Forschung Initiative e.V. (AFI) to H. S., grant TRR 274/12020 (Z01 to Martina Schifferer and Mikael Simons ID 408885537), as well as under Germany's Excellence Strategy within the framework of the AQ6 Munich Cluster for Systems Neurology (EXC 2145 SyNergy ID 390857198; to Martina Schifferer, D. P., and Mikael Simons).

Conflict of interest—The authors declare that they have no conflicts of interest with the contents of this article.

Abbreviations—The abbreviations used are: AD, Alzheimer's disease; APP, amyloid precursor protein; APP FL, full length APP; BSA, bovine serum albumin; CE, cholesterol ester; CTF, C-terminal fragment; EA, erucic acid; ER, endoplasmic reticulum; ESI, electrospray ionisation; FA, fatty acid; FAD, familial AD; FCS, fetal calf serum; NTF, N-terminal fragment; iPSC, induced pluripotent stem cell; PC, phosphatidylcholine; PM, plasma membrane; PS1, presenilin1; TG, triglyceride; TEM, transmission electron microscopy; VLCFA, very long-chain fatty acid.

References

1. Harayama, T., and Riezman, H. (2018) Understanding the diversity of membrane lipid composition. *Nat. Rev. Mol. Cell Biol.* **19**, 281–296
2. Holthuis, J. C., and Menon, A. K. (2014) Lipid landscapes and pipelines in membrane homeostasis. *Nature* **510**, 48–57
3. Casares, D., Escribá, P. V., and Rosselló, C. A. (2019) Membrane lipid composition: effect on membrane and organelle structure, function and compartmentalization and therapeutic avenues. *Int. J. Mol. Sci.* **20**, E2167
4. Phillips, R., Ursell, T., Wiggins, P., and Sens, P. (2009) Emerging roles for lipids in shaping membrane-protein function. *Nature* **459**, 379–385
5. Antonny, B., Vanni, S., Shindou, H., and Ferreira, T. (2015) From zero to six double bonds: phospholipid unsaturation and organelle function. *Trends Cell Biol.* **25**, 427–436
6. Ernst, R., Ejsing, C. S., and Antonny, B. (2016) Homeoviscous adaptation and the regulation of membrane lipids. *J. Mol. Biol.* **428**, 4776–4791
7. Radanović, T., Reinhard, J., Ballweg, S., Pesek, K., and Ernst, R. (2018) An emerging group of membrane property sensors controls the physical state of organellar membranes to maintain their identity. *Bioessays* **40**, e1700250
8. Grimm, M. O., Rothhaar, T. L., and Hartmann, T. (2012) The role of APP proteolytic processing in lipid metabolism. *Exp. Brain Res.* **217**, 365–375
9. Grimm, M. O., Mett, J., Grimm, H. S., and Hartmann, T. (2017) APP function and lipids: a bidirectional link. *Front. Mol. Neurosci.* **10**, 63
10. Bateman, R. J., Xiong, C., Benzinger, T. L., Fagan, A. M., Goate, A., Fox, N. C., *et al.* (2012) Clinical and biomarker changes in dominantly inherited Alzheimer's disease. *N. Engl. J. Med.* **367**, 795–804
11. Kunkle, B. W., Grenier-Boley, B., Sims, R., Bis, J. C., Damotte, V., Naj, A. C., *et al.* (2019) Genetic meta-analysis of diagnosed Alzheimer's disease identifies new risk loci and implicates Aβ, tau, immunity and lipid processing. *Nat. Genet.* **51**, 414–430
12. Steiner, H., Fukumori, A., Tagami, S., and Okochi, M. (2018) Making the final cut: pathogenic amyloid-β peptide generation by γ-secretase. *Cell Stress* **2**, 292–310
13. Scheuner, D., Eckman, C., Jensen, M., Song, X., Citron, M., Suzuki, N., *et al.* (1996) Secreted amyloid β-protein similar to that in the senile plaques of Alzheimer's disease is increased *in vivo* by the presenilin 1 and 2 and APP mutations linked to familial Alzheimer's disease. *Nat. Med.* **2**, 864–870
14. Tang, N., and Kepp, K. P. (2018) Aβ42/Aβ40 ratios of presenilin 1 mutations correlate with clinical onset of Alzheimer's disease. *J. Alzheimers Dis.* **66**, 939–945
15. Braun, G. A., Dear, A. J., Sanagavarapu, K., Zetterberg, H., and Linse, S. (2022) Amyloid-β peptide 37, 38 and 40 individually and cooperatively inhibit amyloid-β 42 aggregation. *Chem. Sci.* **13**, 2423
16. Cullen, N., Janelidze, S., Palmqvist, S., Stomrud, E., Mattsson-Carlgren, N., and Hansson, O. (2022) Association of CSF Aβ38 levels with risk of Alzheimer disease-related decline. *Neurology* **98**, e958–e967
17. De Strooper, B., and Chávez Gutiérrez, L. (2015) Learning by failing: ideas and concepts to tackle γ-secretases in Alzheimer's disease and beyond. *Annu. Rev. Pharmacol. Toxicol.* **55**, 419–437
18. Osenkowski, P., Ye, W., Wang, R., Wolfe, M. S., and Selkoe, D. J. (2008) Direct and potent regulation of γ-secretase by its lipid microenvironment. *J. Biol. Chem.* **283**, 22529–22540
19. Holmes, O., Paturi, S., Ye, W., Wolfe, M. S., and Selkoe, D. J. (2012) Effects of membrane lipids on the activity and processivity of purified γ-secretase. *Biochemistry* **51**, 3565–3575
20. Winkler, E., Kamp, F., Scheuring, J., Ebke, A., Fukumori, A., and Steiner, H. (2012) Generation of Alzheimer disease-associated amyloid β42/43 peptide by γ-secretase can be inhibited directly by modulation of membrane thickness. *J. Biol. Chem.* **287**, 21326–21334
21. Spector, A. A., Kiser, R. E., Denning, G. M., Koh, S. W., and DeBault, L. E. (1979) Modification of the fatty acid composition of cultured human fibroblasts. *J. Lipid Res.* **20**, 536–547
22. Shindou, H., Hishikawa, D., Harayama, T., Yuki, K., and Shimizu, T. (2009) Recent progress on acyl CoA: lysophospholipid acyltransferase research. *J. Lipid Res.* **50 Suppl**, S46–S51
23. Shindou, H., and Shimizu, T. (2009) Acyl-CoA:lysophospholipid acyltransferases. *J. Biol. Chem.* **284**, 1–5
24. Wang, B., and Tontonoz, P. (2019) Phospholipid remodeling in physiology and disease. *Annu. Rev. Physiol.* **81**, 165–188
25. Molenaar, M. R., Jeucken, A., Wassenaar, T. A., van de Lest, C. H. A., Brouwers, J. F., and Helms, J. B. (2019) LION/web: a web-based ontology enrichment tool for lipidomic data analysis. *GigaScience* **8**, giz061
26. Sannerud, R., Esselens, C., Ejsmont, P., Mattera, R., Rochin, L., Tharkeshwar, A. K., *et al.* (2016) Restricted location of PSEN2/γ-secretase determines substrate specificity and generates an intracellular Aβ pool. *Cell* **166**, 193–208
27. Kaether, C., Schmitt, S., Willem, M., and Haass, C. (2006) Amyloid precursor protein and Notch intracellular domains are generated after transport of their precursors to the cell surface. *Traffic* **7**, 408–415
28. Meckler, X., and Checler, F. (2014) Visualization of specific γ-secretase complexes using bimolecular fluorescence complementation. *J. Alzheimers Dis.* **4**, 161–176
29. Yamamoto, T. (1963) On the thickness of the unit membrane. *J. Cell Biol.* **17**, 413–421
30. Ebke, A., Luebbers, T., Fukumori, A., Shirotani, K., Haass, C., Baumann, K., *et al.* (2011) Novel γ-secretase enzyme modulators directly target presenilin protein. *J. Biol. Chem.* **286**, 37181–37186
31. Lands, W. E. (1958) Metabolism of glycerolipides; a comparison of lecithin and triglyceride synthesis. *J. Biol. Chem.* **231**, 883–888
32. Kong, L., Dawkins, E., Campbell, F., Winkler, E., Derks, R. J. E., Giera, M., *et al.* (2020) Photo-controlled delivery of very long chain fatty acids to cell membranes and modulation of membrane protein function. *Biochim. Biophys. Acta Biomembr.* **1862**, 183200
33. Harayama, T., Eto, M., Shindou, H., Kita, Y., Otsubo, E., Hishikawa, D., *et al.* (2014) Lysophospholipid acyltransferases mediate phosphatidylcholine diversification to achieve the physical properties required *in vivo*. *Cell Metab.* **20**, 295–305
34. Valentine, W. J., Yanagida, K., Kawana, H., Kono, N., Noda, N. N., Aoki, J., *et al.* (2021) Update and nomenclature proposal for mammalian lysophospholipid acyltransferases, which create membrane phospholipid diversity. *J. Biol. Chem.* **298**, 101470
35. Robertson, J. D. (1957) New observations on the ultrastructure of the membranes of frog peripheral nerve fibers. *J. Biophys. Biochem. Cytol.* **3**, 1043–1048
36. van Meer, G., Voelker, D. R., and Feigenson, G. W. (2008) Membrane lipids: where they are and how they behave. *Nat. Rev. Mol. Cell Biol.* **9**, 112–124
37. Radde, R., Bolmont, T., Kaeser, S. A., Coomaraswamy, J., Lindau, D., Stoltze, L., *et al.* (2006) Aβ42-driven cerebral amyloidosis in transgenic mice reveals early and robust pathology. *EMBO Rep.* **7**, 940–946
38. Moore, B. D., Martin, J., de Mena, L., Sanchez, J., Cruz, P. E., Ceballos-Diaz, C., *et al.* (2018) Short Aβ peptides attenuate Aβ42 toxicity *in vivo*. *J. Exp. Med.* **215**, 283–301
39. Quartey, M. O., Nyarko, J. N. K., Maley, J. M., Barnes, J. R., Bolanos, M. A. C., Heistad, R. M., *et al.* (2021) The Aβ(1-38) peptide is a negative regulator of the Aβ(1-42) peptide implicated in Alzheimer disease progression. *Sci. Rep.* **11**, 431

40. Petit, D., Fernández, S. G., Zoltowska, K. M., Enzlein, T., Ryan, N. S., O'Connor, A., *et al.* (2022) Aβ profiles generated by Alzheimer's disease causing PSEN1 variants determine the pathogenicity of the mutation and predict age at disease onset. *Mol. Psychiatry* **27**, 2821–2832
41. Liu, L., Lauro, B. M., He, A., Lee, H., Bhattarai, S., Wolfe, M. S., *et al.* (2023) Identification of the Aβ37/42 peptide ratio in CSF as an improved Aβ biomarker for Alzheimer's disease. *Alzheimers Dement.* **19**, 79–96
42. Trambauer, J., Rodríguez Sarmiento, R. M., Fukumori, A., Feederle, R., Baumann, K., and Steiner, H. (2020) Aβ43-producing PS1 FAD mutants cause altered substrate interactions and respond to γ-secretase modulation. *EMBO Rep.* **21**, e47996
43. Steiner, H., Kostka, M., Romig, H., Basset, G., Pesold, B., Hardy, J., *et al.* (2000) Glycine 384 is required for presenilin-1 function and is conserved in bacterial polytopic aspartyl proteases. *Nat. Cell Biol.* **2**, 848–851
44. Steiner, H., Romig, H., Grim, M. G., Philipp, U., Pesold, B., Citron, M., *et al.* (1999) The biological and pathological function of the presenilin-1 Δexon 9 mutation is independent of its defect to undergo proteolytic processing. *J. Biol. Chem.* **274**, 7615–7618
45. Moehlmann, T., Winkler, E., Xia, X., Edbauer, D., Murrell, J., Capell, A., *et al.* (2002) Presenilin-1 mutations of leucine 166 equally affect the generation of the Notch and APP intracellular domains independent of their effect on Aβ42 production. *Proc. Natl. Acad. Sci. U. S. A.* **99**, 8025–8030
46. Paquet, D., Kwart, D., Chen, A., Sproul, A., Jacob, S., Teo, S., *et al.* (2016) Efficient introduction of specific homozygous and heterozygous mutations using CRISPR/Cas9. *Nature* **533**, 125–129
47. Tsugawa, H., Cajka, T., Kind, T., Ma, Y., Higgins, B., Ikeda, K., *et al.* (2015) MS-DIAL: data-independent MS/MS deconvolution for comprehensive metabolome analysis. *Nat. Methods* **12**, 523–526
48. Fahy, E., Sud, M., Cotter, D., and Subramaniam, S. (2007) LIPID MAPS online tools for lipid research. *Nucleic Acids Res.* **35**, W606–W612
49. Jensen, E. B., Gundersen, H. J., and Osterby, R. (1979) Determination of membrane thickness distribution from orthogonal intercepts. *J. Microsc.* **115**, 19–33
50. Schägger, H., and von Jagow, G. (1987) Tricine-sodium dodecyl sulfate-polyacrylamide gel electrophoresis for the separation of proteins in the range from 1 to 100 kDa. *Anal. Biochem.* **166**, 368–379

Edgar Dawkins is a biochemist/neuroscientist specializing in lipids and neurodegenerative diseases. During his PhD at the University of Tasmania, he discovered a phosphoinositide-binding domain in the β-amyloid precursor protein. This led him to pursue further research as a postdoc at LMU Munich, where he developed lipidome engineering strategies to modify γ-secretase activity. He recently started working for Genedata, a software company which develops data infrastructure platforms for the biopharma industry.